

GALAXY POWER SPECTRUM AND BIASING RESULTS FROM THE LOFAR TWO-METRE SKY SURVEY (FIRST DATA RELEASE)

PRABHAKAR TIWARI

National Astronomy Observatories, Chinese Academy of Science, Beijing, 100101, P.R.China

RUIYANG ZHAO

National Astronomy Observatories, Chinese Academy of Science, Beijing, 100101, P.R.China and
University of Chinese Academy of Sciences, Beijing 100049, P.R.China

JINGLAN ZHENG

National Astronomy Observatories, Chinese Academy of Science, Beijing, 100101, P.R.China
University of Chinese Academy of Sciences, Beijing 100049, P.R.China and
Institute of Cosmology and Gravitation, University of Portsmouth, Dennis Sciama Building, Portsmouth PO1 3FX, United Kingdom

GONG-BO ZHAO

National Astronomy Observatories, Chinese Academy of Science, Beijing, 100101, P.R.China and
School of Astronomy and Space Science, University of Chinese Academy of Sciences, Beijing 100049, P.R.China

DAVID BACON

Institute of Cosmology and Gravitation, University of Portsmouth, Dennis Sciama Building, Portsmouth PO1 3FX, United Kingdom

DOMINIK J. SCHWARZ

Fakultät für Physik, Universität Bielefeld, Postfach 100131, 33501 Bielefeld, Germany
Draft version April 9, 2021

Abstract

The LOFAR Two-metre Sky Survey (LoTSS) is ongoing and plans to map the complete Northern sky in the future. The source catalogue from the public LoTSS first data release covers 1% of the sky and is known to show some correlated noise or fluctuations of the flux density calibration over a few degree scale. Due to its unique and excellent design, observations from LOFAR are expected to be an excellent opportunity to study the distribution and evolution of the large-scale structure of the Universe in the future. We explore the LoTSS DR1 to understand the survey systematics and data quality of its very first data release. We produce catalog mocks to determine error estimates and with our detailed and careful analysis, we successfully recover the angular clustering statistics of LoTSS galaxies, which fits the Λ CDM cosmology reasonably well. We employ a Markov chain Monte Carlo (MCMC) based Bayesian analysis and recover the best galaxy biasing scheme for LoTSS galaxies and also constrain the radial distribution of LoTSS DR1. After masking some noisy and uneven patches and with reasonable flux cuts, the LOFAR survey appears qualified for large-scale cosmological studies. The upcoming data releases from LOFAR are expected to be deeper and wider, thus will be more suitable for drawing cosmological implications.

Subject headings: cosmology: large-scale structure of universe – dark matter – galaxies: active – high-redshift

1. INTRODUCTION

Our present understanding of the origin and evolution of the Universe is based on the Lambda cold dark matter (Λ CDM) cosmology. The matter density of the Universe is dominated by the CDM, whose gravitational evolution results in a population of virialized dark matter halos of different masses (Press & Schechter 1974; Scherrer & Bertschinger 1991; Navarro et al. 1997; Ma & Fry 2000; Seljak 2000; Scoccimarro et al. 2001; Cooray & Sheth 2002). The formation of galaxies occurs inside these dark matter halos and the host halo mass and its evolution

roughly determines the evolution and type (Girelli et al. 2020) of galaxy residing inside. In general, the radio-loud galaxy's active galactic nuclei (AGNs) are found to reside in more massive halos than optical AGNs (Mandelbaum et al. 2009; Wilman et al. 2008). That being so, the visible and radio observations sample quite a different set of galaxies (halos). Most bright galaxies (in visible) are undetectable at radio wavelengths, and most strong radio sources are optically faint or invisible. The radio surveys are towards the higher end of the halo mass range as compared with visible/IR observation and thus are essential and complement best the existing and upcoming visible/IR galaxy surveys (Kauffmann et al. 2003; Best et al. 2005; Mandelbaum et al. 2009; Best et al. 2014;

Nusser & Tiwari 2015; Krumpel et al. 2018; Hale et al. 2018; Alonso et al. 2020; Lan & Prochaska 2021; Wolf et al. 2021).

The international Low-Frequency Array (LOFAR; van Haarlem et al. 2013), a new-generation radio interferometer constructed in northern Netherlands and across Europe, is an excellent radio instrument offering transformational increase in radio survey speed with unparalleled sensitivity and angular resolution in the low-frequency radio regime (Röttgering et al. 2003; van Haarlem 2005; Röttgering et al. 2005; Falcke et al. 2007). The LOFAR Two-metre Sky Survey (LoTSS) is a deep 120–168 MHz imaging survey which is ongoing and being carried out using LOFAR high-band antenna (HBA) observations across the whole northern hemisphere (Shimwell et al. 2017, 2019). The LoTSS is mainly aiming to explore the large-scale structure, galaxies, cluster of galaxies and formation and evolution of massive black holes. The LoTSS survey will observe millions of radio AGNs, along with a significant number of star-forming galaxies (SFGs) out to the redshift $z \sim 6$, allowing detailed studies of the physics of AGNs, SFGs and their evolution. The LoTSS is producing high-fidelity images at central frequency of 144 MHz with a resolution of 6 arcsec and with declination-dependent sensitivity, typically around $100 \mu\text{Jy}/\text{beam}$. This is a factor of 10 more sensitive than the current best high-resolution sky survey, e.g., VLA’s FIRST. LoTSS will finally detect over 10 million radio sources, mostly AGNs but with a significant fraction of star-forming galaxies. A large fraction of LoTSS sources will have optical identifications and photometric redshifts will be available (Williams et al. 2019; Duncan et al. 2019). Furthermore, the WHT Enhanced Area Velocity Explorer (WEAVE) multi-object spectrograph on the William Herschel Telescope will observe optical (370–970 nm) spectra of millions of LOFAR radio sources and provide precise redshift information (Smith et al. 2016). Loaded with the most advanced features, speed, sensitivity and photo+spectroscopic redshifts, the LoTSS survey is expected to provide an excellent opportunity for astrophysical and cosmological studies.

The LoTSS survey, homogeneously covering the whole northern sky complete down to the sub mJy limit will eventually observe around 15 million radio sources and will overcome statistical limitations due to shot noise. The large galaxy number density will substantially reduce cosmic variance in cosmological analysis. The radio galaxies, tracing the background dark matter, will constrain the shape of power spectrum, i.e., the early universe physics, dark matter, baryon, and neutrino densities, the inflation power spectrum and the degree of non-Gaussianity in density fluctuations. The upcoming LoTSS catalogs, covering a large sky area, will help us to explore further on large-scale anomalies (de Oliveira-Costa et al. 2004; Ralston & Jain 2004; Schwarz et al. 2004; Tiwari & Aluri 2019) and current puzzling dipole signal observed with radio catalogs (Singal 2011; Rubart & Schwarz 2013; Tiwari et al. 2015; Tiwari & Jain 2015; Tiwari & Nusser 2016; Ghosh et al. 2016; Bengaly et al. 2018; Maartens et al. 2018; Agarwal et al. 2019; Qiang et al. 2020; Bengaly et al. 2019; Secrest et al. 2020; Siewert et al. 2020b; Das et al. 2021). Furthermore, LoTSS will significantly improve on present low-frequency radio catalog, e.g., TIFR GMRT Sky Survey (TGSS; In-

tema et al. 2017) and GaLactic and Extragalactic All-sky MWA (GLEAM; Hurley-Walker et al. 2017), and analysis based on these surveys (Tiwari 2019; Rana & Bagla 2019; Dolfi et al. 2019; Tiwari et al. 2019; Choudhuri et al. 2020). Unfortunately, the link between the galaxy power spectrum and background matter depends on some unknowns from astrophysics such as the galaxy bias factor which depends on galaxy type and is quite different for radio AGNs and star-forming galaxies. The LoTSS population is mixed, i.e., radio AGNs + star-forming galaxies and therefore understanding galaxy bias, their relative number densities and luminosity evolution is non-trivial. The purpose of this work is to present a detailed cosmological analysis of LoTSS galaxies and study the effect of survey footprint, shot-noise and other systematics. We have produced galaxy mocks for survey and customized and calibrated the data pipeline for galaxy clustering statistics recovery.

We introduce the present available catalog, i.e., LoTSS DR1, its completeness and data mask in Section 2 and 2.1. In Section 3, we present mock generation details and co-variance matrix estimations. We briefly present the theoretical formulation of galaxy angular power spectrum estimate and its connection to background dark matter power spectrum in Section 4. In Section 5 and 6, we present our measured angular power spectrum and two-point correlation statistics, respectively. We present an estimate for the bias for LoTSS population in Section 7 and summarize our results in Section 8. We conclude with discussion in Section 9.

2. LOTSS DR1 CATALOG

The LOFAR Two-metre Sky Survey (LoTSS; Shimwell et al. (2017)) is ongoing and planned to scan the entire northern sky at 120-168 MHz. Shimwell et al. (2019) prepare the first full-quality public data release (LoTSS-DR1) catalog from 63 LoTSS data sets (2% of the total survey) in the region of the HETDEX Spring Field that were observed between 2014 May 23 and 2015 October 15. The LoTSS DR1 been prepared using a fully automated direction-dependent calibration and imaging pipeline discussed in Shimwell et al. (2017). The catalog covers 424 square degrees and contains total 325,694 sources with peak flux density at least five times the local rms noise, thus a source density of about 770 sources per square degree. The resolution of the survey images is 6 arcsec and the positional accuracy of the sources in catalog is within 0.2 arcsec. The median sensitivity is $71 \mu\text{Jy}/\text{beam}$ at 144 MHz. Williams et al. (2019) remove artefacts and corrects wrong groupings of Gaussian components and prepare a value-added catalog, the catalog then contains 318,520 point sources of which 231,716 have optical/near-IR identifications in Pan-STARRS¹/WISE², not all of these have photo- z detection, as Pan-STARRS is not as complete as WISE and we only have photo- z ’s for about 50% of all radio sources.

2.1. Completeness and data mask

Shimwell et al. (2019) estimate the completeness of LoTSS-DR1 and report the catalog to be 65% at 0.23

¹ <https://www.ifa.hawaii.edu/research/Pan-STARRS.shtml>

² https://www.nasa.gov/mission_pages/WISE/main/index.html

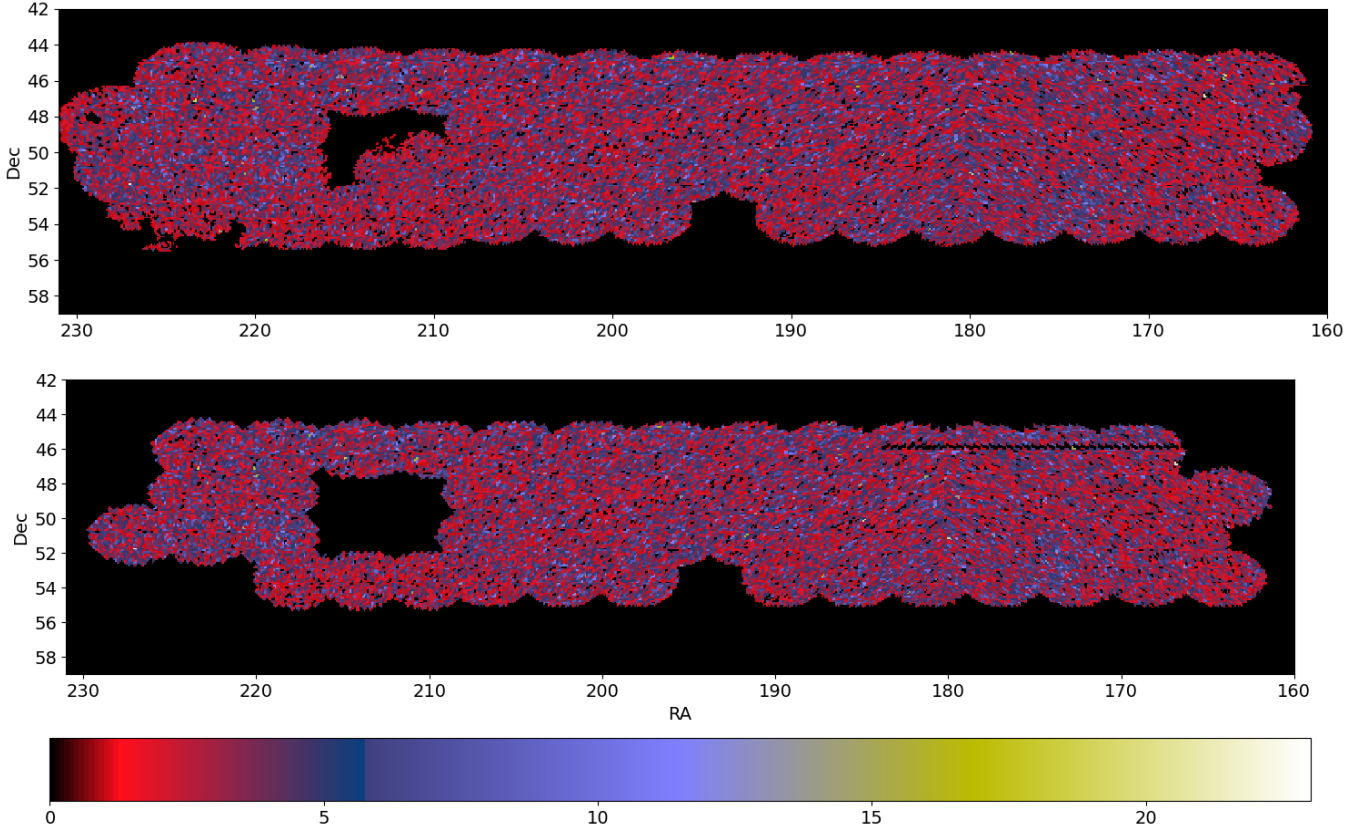


FIG. 1.— The distribution of radio galaxies in the LoTSS-DR1 catalog with integrated flux density between 1 to 10,000 mJy. Plotted are the number counts in pixels in Cartesian projection at HEALPix resolution $N_{\text{side}} = 512$ before (top) and after (bottom) applying the mask. After applying mask and 1 to 10,000 mJy flux cut there remains 107, 926 sources only.

mJy, 90% at 0.45 mJy, and 95% complete at 0.58 mJy. The catalog is almost complete at 1 mJy. The LoTSS DR1 catalogue was generated by combining 58 individual LOFAR pointings on the sky, and due to poor ionospheric conditions and due to the presence of bright sources the imaging pipeline occasionally produces sub-standard images. As a result some pointings show in-homogeneous point source distribution, for example, 5 pointings show significant incompleteness (Siewert et al. 2020a). After properly defining the survey region and masking 5 incomplete pointings a reasonable survey mask (mask-z) for reliable cosmology is shown in figure 2. Mask-z³ is an upgrade to mask-d, it rejects regions of equal declination, where information of Pan-STARRS is missing in addition to mask-d. Mask-d is originally given and described in Siewert et al. (2020a). We impose the completeness flux cut (i.e., 1 mJy) and also remove the ultra bright sources with flux equal or greater than 10 Jy, the catalog thus contains 121,730 sources. Next we mask pointings with systematics and employ a survey geometry mask shown in figure 2, there remains 107,926 sources only.

3. MOCK CATALOGS AND CO-VARIANCE MATRIX ESTIMATION

Mock catalogues are essential for assessing analysis pipeline, and data systematics and errors in the cosmo-

³ We thank Thilo Siewert for preparing and making mask-z available to us.

logical analysis of large galaxy surveys. In order to estimate the uncertainty in cosmological signal recovered from LoTSS data we generate 1000 LoTSS mocks of the large scale structure by employing the lognormal (and Gaussian) density field simulator code FLASK⁴ (Xavier et al. 2016). To emulate the LoTSS DR1 catalog, we generate multiple lognormal density fields tomographically in 35 redshift slices (0 to redshift 3.5), each with a width $\Delta z = 0.1$. All statistical properties (i.e., auto and cross-correlations) are determined by the input angular power spectrum. In addition, effects including the redshift-space distortions and lensing are also counted in the simulation via the input spectra provided to the FLASK pipeline.

The input theoretical angular power spectrum, C_ℓ , in different redshift bins are generated using CAMB (Challinor & Lewis 2011) which includes the effects on the observed number counts of redshift-space distortions and lensing. The redshift distribution profile $n(z)$ is provided along with C_ℓ s to FLASK to generate mock number count maps. Computation of theoretical C_ℓ requires a galaxy bias, $b(z)$, we assume the NVSS best fit bias (Nusser & Tiwari 2015) and generate mock LoTSS DR1 catalogs. We assume a Λ CDM model and use Planck Collaboration et al. (2018) cosmological parameters as the fiducial cosmology.

We apply the LoTSS DR1 survey mask to precisely count for survey geometry and then from the mock

⁴ <http://www.astro.iag.usp.br/flask/>

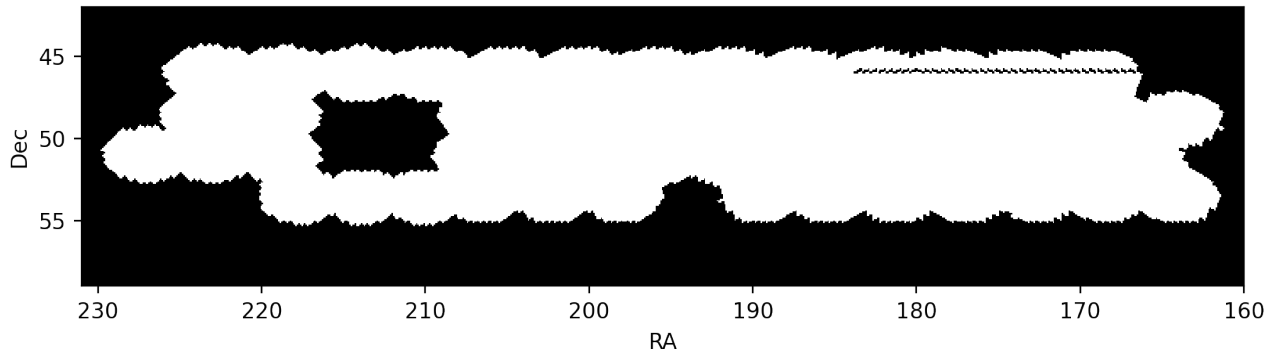


FIG. 2.— LoTSS DR1 mask-z. The mask rejects 5 under-sampled pointings and includes all 53 good pointings of LOFAR HETDEX field. Also it rejects regions of equal declination, where information of Pan-STARRS is missing. The mask been prepared considering the survey geometry, consistency of source count, sampling uniformity etc., (Siewert et al. 2020a).

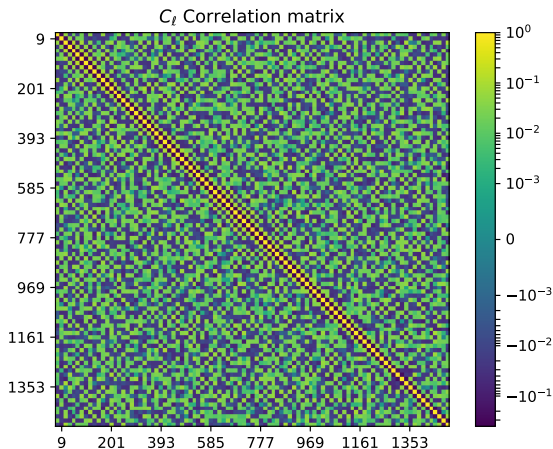


FIG. 3.— Angular power spectrum correlation matrix constructed from 1000 mocks. The galaxy mocks generated using FLASK log-normal density simulator. Each galaxy mock follows the same sky coverage and contains roughly the same number of sources as LoTSS DR1 after mask and flux cuts.

catalogs, we calculate angular power spectrum up to $l \approx 1500$. Although LoTSS DR1 is a relatively high number density radio catalog, it is hardly over 1% of the sky, and therefore, given the small sky coverage, C_ℓ is noisy so we choose $\Delta\ell = 16$ and recover C_ℓ s in bands by collecting 16 multipoles per bin. Finally, with mock C_ℓ s, we compute a covariance matrix to determine the uncertainty in LoTSS DR1 recovered galaxy power. A plot of correlation matrix of angular power spectrum is shown in figure 3.

4. GALAXY ANGULAR POWER SPECTRUM

The galaxies are the biased tracers of the background dark matter density and thus the background cosmological model. The theoretical formulation of the background matter density perturbations to galaxy density are easily written in terms of galaxy clustering measures. The statistical measure of clustering of galaxies

can be conventionally expressed in terms of the angular power spectrum, C_ℓ . Following the Λ CDM scenario, the theoretical formulation of C_ℓ in brief is as follows. Assume a uniform galaxy survey catalog with an area \mathcal{A} and total number of galaxies \mathcal{N} . The mean number density, $\bar{\mathcal{N}}$, per steradian is thus simply \mathcal{N}/\mathcal{A} . Subsequently, $\mathcal{N}(\hat{\mathbf{r}}) = \bar{\mathcal{N}}(1 + \Delta(\hat{\mathbf{r}}))$, be the projected number density per steradian in the direction $\hat{\mathbf{r}}$. Here $\Delta(\hat{\mathbf{r}})$ is the projected number density contrast and theoretically connected to the background matter density contrast, $\delta_m(\mathbf{r}, z(r))$. Note that \mathbf{r} stands for comoving distance r in direction $\hat{\mathbf{r}}$ and $z(r)$ is the redshift corresponding to comoving distance r . The galaxy density contrast, $\delta_g(\mathbf{r}, z(r))$, in the direction $\hat{\mathbf{r}}$ and at redshift z , in terms of matter density contrast $\delta_m(\mathbf{r}, z(r))$,

$$\delta_g(\mathbf{r}, z(r)) = \delta_m(\mathbf{r}, z=0)D(z)b(z), \quad (1)$$

where $b(z)$ is galaxy biasing, $D(z)$ is the linear growth factor. Following these we can formulate the theoretical $\Delta(\hat{\mathbf{r}})$,

$$\begin{aligned} \Delta(\hat{\mathbf{r}}) &= \int_0^\infty \delta_g(\mathbf{r}, z(r))p(r)dr \\ &= \int_0^\infty \delta_m(\mathbf{r}, z=0)D(z)b(z)p(r)dr, \end{aligned} \quad (2)$$

where $p(r)dr$, the radial distribution function, is the probability of observing galaxy between comoving distance r and $(r + dr)$. Note that the $\Delta(\hat{\mathbf{r}})$ may also have some tiny additional contributions from lensing, redshift distortions, physical distance fluctuations and from variation of radio source luminosities and spectral indices (Chen & Schwarz 2015). Although, these effects are still expected to be limited to few percent on the largest scales (Dolfi et al. 2019). Next, we expand $\Delta(\hat{\mathbf{r}})$ in terms of spherical harmonics to obtain C_ℓ ,

$$\Delta(\hat{\mathbf{r}}) = \sum_{\ell m} a_{\ell m} Y_{\ell m}(\hat{\mathbf{r}}). \quad (3)$$

We use the orthonormal property of spherical harmon-

ics and write $a_{\ell m}$ as,

$$\begin{aligned} a_{\ell m} &= \int d\Omega \Delta(\hat{\mathbf{r}}) Y_{\ell m}^*(\hat{\mathbf{r}}) \\ &= \int d\Omega Y_{\ell m}^*(\hat{\mathbf{r}}) \int_0^\infty \delta_m(\mathbf{r}, z=0) D(z) b(z) p(r) dr. \end{aligned} \quad (4)$$

We can Fourier transform the matter density field $\delta_m(\mathbf{r}, z=0)$ and write $a_{\ell m}$ as,

$$a_{\ell m} = \frac{i^\ell}{2\pi^2} \int dr D(z) b(z) p(r) \int d^3k \delta_{\mathbf{k}} j_\ell(kr) Y_{\ell m}^*(\hat{\mathbf{k}}). \quad (5)$$

Subsequently, we find the expression for angular power spectrum, C_ℓ , as,

$$\begin{aligned} C_\ell &= \langle |a_{\ell m}|^2 \rangle \\ &= \frac{2}{\pi} \int dk k^2 P(k) \left| \int_0^\infty D(z) b(z) p(r) dr j_\ell(kr) \right|^2 \\ &= \frac{2}{\pi} \int dk k^2 P(k) W^2(k), \end{aligned} \quad (6)$$

where $P(k)$ is Λ CDM power spectrum, $W(k) = \int_0^\infty D(z) b(z) p(r) dr j_\ell(kr)$ is the k -space window function. The galaxies are discrete point sources and thus the measured angular power spectrum of a galaxy catalog incorporates the Poissonian shot-noise contribution $\frac{1}{N}$. Therefore, the observed power spectrum C_ℓ^{obs} corresponding to the theoretical C_ℓ given in Equation (6) is $C_\ell^{\text{measured}} - \frac{1}{N}$. The uncertainty in C_ℓ determination due to cosmic variance, sky coverage and shot-noise is,

$$\Delta C_\ell = \left(\frac{2}{(2\ell + 1) f_{\text{sky}}} \right)^{1/2} C_\ell^{\text{measured}}, \quad (7)$$

where f_{sky} is the fraction of sky covered by survey.

5. C_ℓ MEASUREMENTS

We make use of a pseudo- C_ℓ recovery algorithm by Alonso et al. (2019) to achieve an efficient and reasonably accurate estimate of the angular power spectrum of LoTSS DR1 catalog. The algorithm python module is publicly available as NaMaster⁵, and the mathematical background of the estimator, its features, and its software implementation are described in Alonso et al. (2019). We test the performance of pseudo- C_ℓ algorithm for LoTSS DR1 mask with a test map, which resembles the LoTSS DR1 density fluctuations, and obtain a reasonable recovery of C_ℓ 's by using an un-apodized mask shown in figure 2. To emulate the LoTSS DR1 catalog, we first generate $a_{\ell m}$ using LoTSS DR1 model C_ℓ 's⁶, subsequently we obtain a density contrast map from $a_{\ell m}$ by making use of spherical harmonics (equation 3). Next, we apply the LoTSS DR1 mask to this test map and recover $C_{\ell S}$ (pseudo- $C_{\ell S}$). The results thus obtained with different configurations and settings are shown in figure 4 and above $\ell > 100$, a reasonable recovery is demonstrated.

With above demonstrated settings, we run the pseudo- C_ℓ recovery algorithm and obtain LoTSS DR1 catalog angular power spectrum. The angular spectrum thus

obtained is shown in figure 5. The recovered power spectrum for galaxies with integrated radio flux above survey completeness, i.e., $S > 1$ mJy roughly agrees with theoretical results obtained following Λ CDM and considering NVSS (Condon et al. 1998) radio galaxy biasing and radial distribution (Nusser & Tiwari 2015). Without considering survey completeness (i.e., the flux cut) the recovered power spectrum is significantly high at low ℓ , i.e., at large scales, presumably attributing the effect of survey incompleteness. Considering slightly higher flux cut, i.e. $S > 2$ mJy, we roughly obtain the same, $S > 1$ mJy flux cut $C_{\ell S}$ but with slightly more fluctuations.

6. 2-POINT CORRELATION STATISTICS

For comparison with theory and earlier results in Siewert et al. (2020a), we calculate 2-point correlation function (2PCF) for LoTSS DR1 catalogue. We obtain approximately the same 2PCF results with our catalog and mask, as in Siewert et al. (2020a) with 1 mJy flux cut and their mask-d. The theoretical curve at angular scales less than 0.1 degree is slightly lower than the measured values, presumably due to multi-component nature of a few radio sources. We have followed Siewert et al. (2020a) and applied the same python package TreeCorr⁷ (Version 4.0) (Jarvis et al. 2004) and the same parameter settings for 2PCF estimation. However, our mask-z additionally masks a strip where information of Pan-STARRS is missing. Following Siewert et al. (2020a) we next divide LoTSS DR1 catalogue into three patches 'left', 'center' and 'right'. The RA ranges for these patches are 161-184, 184-208, and 208-230 degrees, respectively. The calculated angular correlation functions are shown in figure 6. We find that the center area fits the theory best. The slight mismatch between 'left', 'center' and 'right' patches is an indication of large scale density fluctuation systematics present in data. This should be considered as a motivation for refining LoTSS DR1 pipeline (Shimwell et al. 2019).

7. GALAXY BIAS AND $N(z)$ ESTIMATE

The bias $b(z)$ for each galaxy population is different and depends on dark matter halo mass hosting the galaxy type (Mo & White 1996). Although, the angular power spectrum of LoTSS DR1 in figure 4 apparently a close match with Λ CDM estimates considering NVSS galaxies bias and redshift distribution, $N(z)$. However, in reality, the bias and $N(z)$ for LoTSS DR1 galaxies could be significantly different in comparison with values obtained for NVSS galaxies with flux above 10 mJy (NVSS completeness) at 1.4 GHz (Nusser & Tiwari 2015; Tiwari & Nusser 2016). The NVSS is dominantly radio loud AGNs, Fanaroff-Riley type I (FR I) and FR II (Fanaroff & Riley 1974), whereas the LoTSS DR1 above 1 mJy (completeness) presumably dominantly contains star-forming galaxies along with radio loud AGNs, FR I and FR II type (Calistro Rivera et al. 2017; Wilman et al. 2008). The LoTSS DR1 population is mixed and differs from NVSS, and thus the bias $b(z)$ and $N(z)$ could significantly be different. For $N(z)$, around half of the LoTSS DR1 sources have optical/near-IR identification in Pan-STARRS/WISE and their photometric redshifts

⁵ <https://namaster.readthedocs.io/en/latest/index.html>

⁶ C_ℓ is the expected variance of the $a_{\ell m}$ at ℓ .

⁷ <http://github.com/rmjarvis/TreeCorr/>

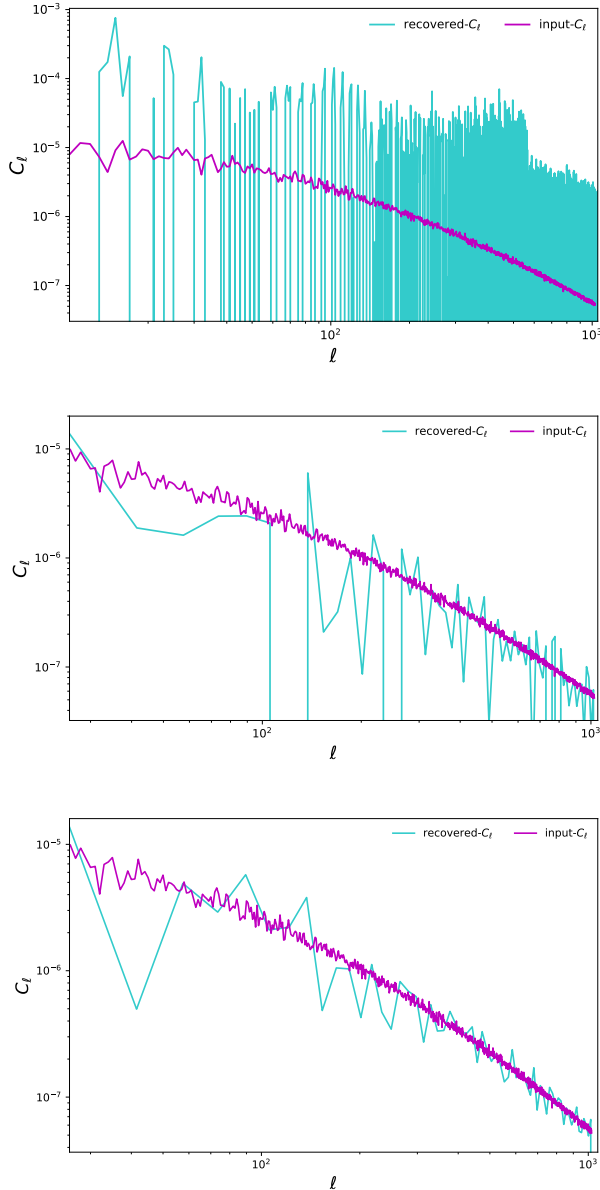


FIG. 4.— Angular power spectrum recovery performance with LoTSS DR1 mask (0.1% of the sky!). The recovered power spectrum is significantly fluctuating with multipoles (top figure). Next we apodized mask on the scale of one degree and plot C_ℓ s in bands by collecting 16 multipoles per bin. In the middle figure above we have shown the results, this shows somewhat better recovery. The best recovery above $\ell > 100$ is obtained if we do not apodized mask and collect 16 multipoles per bin (bottom figure).

are available. The number count of these photo identified galaxies in redshift bins ($\Delta z = 0.1$) is shown in figure 7. Note that the $N(z)$ in figure 7 is only representing partial LoTSS DR1 population; the true $N(z)$ of the full LoTSS DR1 catalog could be significantly different. Nevertheless, the available photo-redshifts can be assumed to loosely represent the full LoTSS DR1 galaxies’ redshift distribution.

Assuming a Λ CDM cosmology we seek to constrain the galaxy bias $b(z)$ and radial distribution $N(z)$ of LoTSS DR1 galaxies by fitting measured angular power spectrum in figure 5 and observed $N(z)$ photo- z histogram

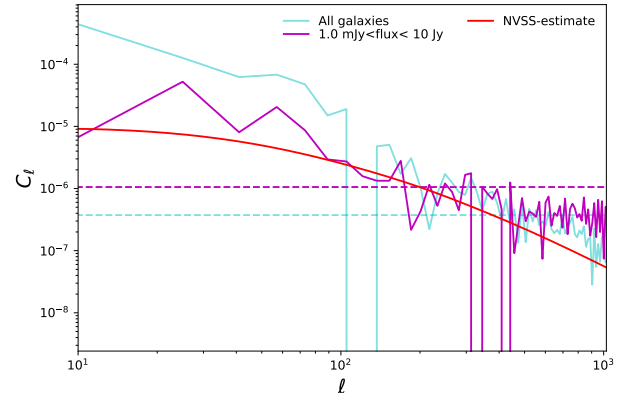


FIG. 5.— LoTSS DR1 angular power spectrum recovery. We obtain approximate theoretical power spectrum ‘NVSS-estimate’ for LoTSS DR1 catalog following equation 6 and assuming NVSS galaxy bias and redshift distribution (Nusser & Tiwari 2015). The power spectrum obtained without flux cut is significantly high at large scales (low ℓ). The LoTSS DR1 catalog is only expected to be complete above 1 mJy.

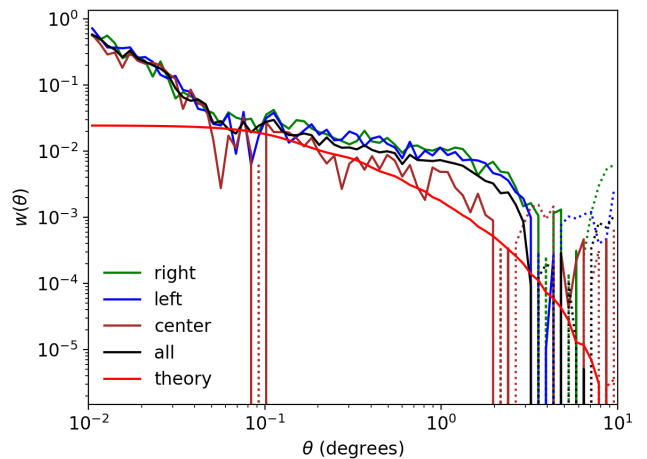


FIG. 6.— The 2-point correlation function of LoTSS DR1 catalogs in different patches of the sky. Green curve denotes the ‘right’ patch angular correlation function, the blue for ‘left’ area and orange for ‘center’ area. The whole area angular correlation function of LoTSS DR1 is shown in black line, while the red curve denotes the theoretical prediction following Λ CDM with NVSS bias and redshift distribution. All dotted lines represent negative values.

in figure 7. For a given bias, $b(z)$ and $N(z)$ we calculate theoretical (model) angular power spectrum C_ℓ^{th} . Next we obtain the likelihood, i.e., the probability to have observed data C_ℓ^{obs} given the model, $\mathcal{P}(C_\ell^{\text{obs}}|b(z), N(z)) \propto \mathcal{L}(C_\ell^{\text{obs}}) \propto \exp(-\frac{1}{2}(C_\ell^{\text{obs}} - C_\ell^{\text{th}})^T \Sigma^{-1}(C_\ell^{\text{obs}} - C_\ell^{\text{th}}))$. Here Σ is the co-variance matrix computed using mocks discussed in Section 3. We make use of Bayes’ probability theorem⁸, and write the model probability given the data, $\mathcal{P}(b(z), N(z)|C_\ell^{\text{obs}}) = \mathcal{P}(C_\ell^{\text{obs}}|b(z), N(z)) \times \mathcal{P}(b(z))$. Here $\mathcal{P}(b(z))$ is the prior probabilities of bias $b(z)$.

We assume different $N(z)$ templates and run MCMC sampler to maximize model parameters probability,

⁸ $P(A|B)P(B) = P(B|A)P(A)$

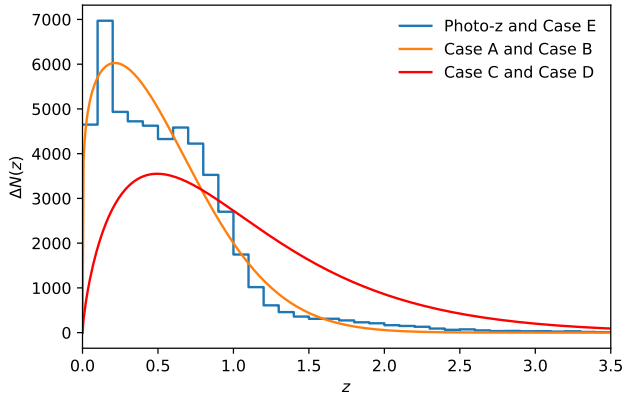


FIG. 7.— Number of radio sources per redshift bin $\Delta z = 0.1$ of available z for flux density thresholds $S > 1$ mJy. The redshift distributions recovered by fitting Λ CDM cosmology are also shown.

$\mathcal{P}(b(z), N(z)|C_\ell^{\text{obs}})$, i.e., obtain best fit to Λ CDM cosmology and deduce effective bias $b(z)$, given the $N(z)$ values. We conveniently use Cobaya (Torrado & Lewis 2020) to perform Bayesian analysis and CosmoMC (Lewis & Bridle 2002; Lewis 2013) for MCMC sampling. With mock catalogs, we verify above MCMC pipeline and recover the input bias within one sigma uncertainty. We would like to emphasize that the measured C_ℓ 's are projected quantities, and it is hard to extract tomographic information from it. The recovered bias is strongly dependent on $N(z)$ assumption. Even so, assuming a variety of $N(z)$ is something best we can do for now for LoTSS catalog. We hope to have better $N(z)$ observations in future and thus better constraints on $b(z)$.

Case A: Assuming the parametric form of $N(z) \propto z^{a_1} \exp\left[-\left(\frac{z}{a_2}\right)^{a_3}\right]$ given in Nusser & Tiwari (2015) we fit the observed photo- z histogram in figure 7 and obtained a_1, a_2, a_3 as 0.16, 0.82, 1.84, respectively. The $N(z)$ thus obtained is shown in figure 7. Next, we assume a redshift independent bias, i.e., $b(z) = b_{\text{eff}}$ and fit with recovered LoTSS DR1 angular power spectrum. We obtain that a bias $b_{\text{eff}} = 2.19^{+0.15}_{-0.14}$ fits best with the data. The recovered best power spectrum is shown in figure 11.

Case B: $N(z)$ parametric form same as in case A. And for galaxy bias we assume quadratic dependence over redshift, i.e., $b(z) = b_0 + b_1z + b_2z^2$. As we are fitting angular power spectrum C_ℓ , i.e., projected clustering statistics in 2D angular space, we are effectively only constraining integrated $\sim b^2(z)N^2(z)$, and therefore observe a large degeneracy between b_0, b_1, b_2 . To check how well quadratic bias obtained in Nusser &

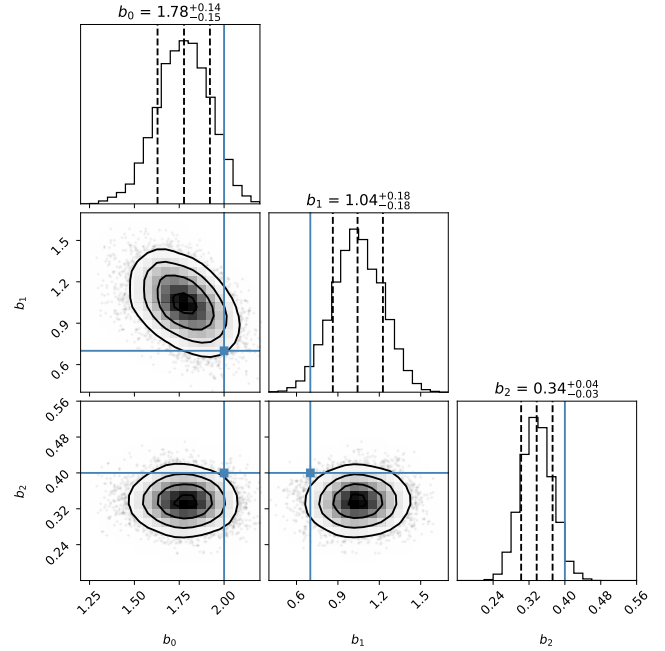


FIG. 8.— Case B: The MCMC sampler results showing the one and two-dimensional posterior distributions for each free parameter. The cyan color solid lines show the initial reference point of MCMC sampler. The results do not depend on starting point. A broad Gaussian prior (see Table 1) is used for bias free parameters b_0, b_1, b_2 .

Tiwari (2015) fits with LoTSS DR1⁹, we assume a Gaussian prior for b_0, b_1, b_2 with large variances. The bias $b(z)$ thus recovered is slightly higher than NVSS. The MCMC sampler results are shown in figure 8, and the best fit power spectrum is in figure 11.

Case C: Assume $N(z) \sim z^{0.74} \exp\left[-\left(\frac{z}{0.71}\right)^{1.1}\right]$ schemes given in Nusser & Tiwari (2015) we fit a quadratic bias $b(z) = b_0 + b_1z + b_2z^2$. The best bias, $b(z)$, and angular power spectrum thus recovered is shown in figure 10 and 11, respectively. The bias recovered is larger than case B and NVSS. The MCMC sample and posterior distributions are shown in figure 9.

Case D: $N(z)$ same as in case C, and we use an effective redshift independent bias. We obtain that a bias $b_{\text{eff}} = 3.31 \pm 0.07$ fits best with data. The recovered best fit angular power spectrum is shown in figure 11.

Case E: We assume the observed photo- z

⁹ However, note that the LoTSS population is mixed and dominantly the star-forming galaxies are in the catalog, whereas the NVSS population studied in Nusser & Tiwari (2015) and Tiwari & Nusser (2016) consists of AGNs only!

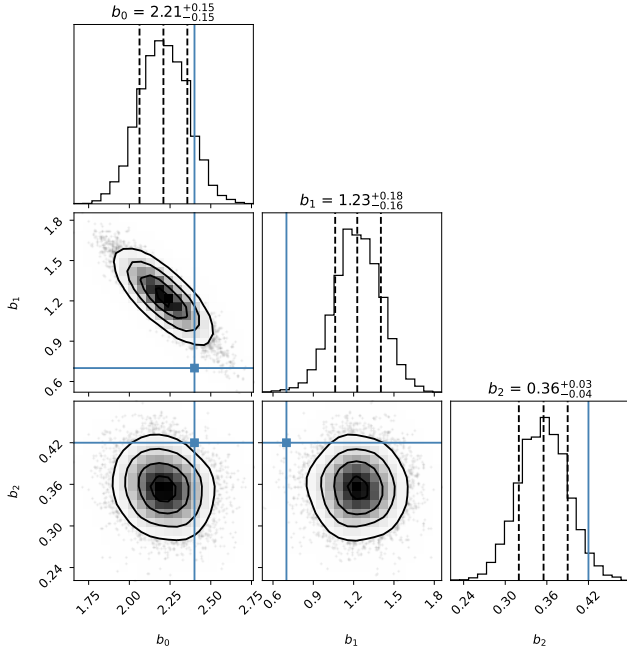


FIG. 9.— Case C: One and two-dimensional posterior distributions of quadratic bias free parameters b_0 , b_1 , b_2 . A Gaussian prior with large variance is used for each bias parameter b_0 , b_1 , b_2 . Other details same as in figure 8.

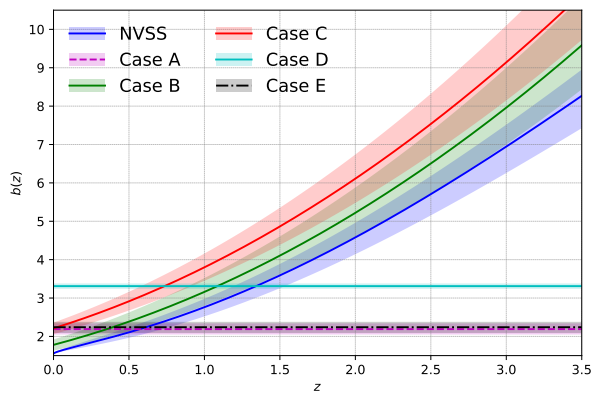


FIG. 10.— The bias, $b(z)$, recovered with MCMC Bayesian fitting for different cases. The best bias for NVSS radio AGNs obtained in (Nusser & Tiwari 2015) is also shown.

histogram¹⁰ in figure 7 representing full-LoTSS population and run MCMC sampler to find the best redshift independent bias value. We obtain $b_{\text{eff}} = 2.24^{+0.14}_{-0.15}$ best fits the data. The best fit angular power spectrum and bias with one sigma uncertainty band is shown in figure 11 and 10, respectively.

8. SUMMARY

¹⁰ a cubic spline interpolation is used to make $N(z)$ smoother.

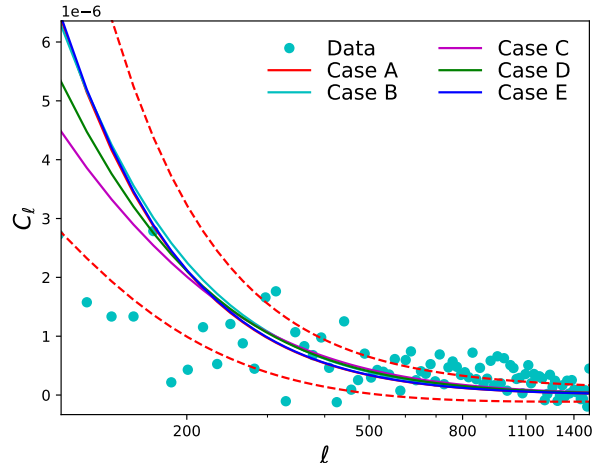


FIG. 11.— The best Λ CDM C_ℓ obtained using Bayesian MCMC sampling with various set of bias, $b(z)$ and $N(z)$ constraints and assumptions as discussed in Section 7. The estimated observed pseudo- C_ℓ from data are also shown. The red color dashed curves show the one sigma limit due to shot-noise and cosmic variance following equation 7 for case A. For other cases the one sigma limit curves are roughly the same.

We explore the first data release of LOFAR survey for cosmological studies. We generate detailed data mocks and construct co-variance matrix for angular power spectrum recovery. With our mocks, we are able to customise the settings of pseudo angular power recovery algorithm for LoTSS. The LoTSS DR1 contains dominantly star-forming galaxies and a significant fraction of AGNs, therefore, the resultant bias and radio distribution of galaxies can't be naively assumed the same as seen with other radio surveys with high flux limit, e.g., the NVSS, where the catalog entirely almost consists of AGNs. We have explored the galaxy bias and possible radial distribution profiles for LoTSS galaxies and have presented their relative fits with data. For convenience, the summary of different cases, the recovered bias with fit quality parameters, i.e., χ^2/dof , and the model selection criteria parameters the Akaike's information criterion (AIC) and Bayesian information criterion (BIC) are listed in Table 1.

We try fitting the best bias and $N(z)$ profiles from NVSS (Nusser & Tiwari 2015; Tiwari & Nusser 2016) to LoTSS and obtain that the bias for LoTSS DR1 is slightly higher in comparison with NVSS if we assume NVSS $N(z)$ (Case C). Our bias values are also slightly higher in comparison with Alonso et al. (2020) bias results, ob-

TABLE 1
MCMC SAMPLER RESULTS. THE PRIOR AND BEST VALUE OF THE MODEL FREE PARAMETERS AND UNCERTAINTIES. THE FLAT PRIOR RANGE IS SHOWN IN SQUARE BRACKETS, AND $\mathcal{N}(\mu, \sigma)$ DENOTES THE GAUSSIAN PRIOR WITH MEAN μ AND STANDARD DEVIATION σ . THE REDUCED χ^2 , I.E., χ^2 PER DEGREES OF FREEDOM, AIC AND BIC ARE ALSO LISTED FOR MODEL FIT COMPARISON.

		Case A	Case B	Case C	Case D	Case E
b_0	prior		$\mathcal{N}(1.6, 0.64)$	$\mathcal{N}(1.6, 0.64)$		
	fit value	–	$1.78^{+0.14}_{-0.15}$	$2.21^{+0.15}_{-0.15}$	–	–
b_1	prior		$\mathcal{N}(0.85, 0.17)$	$\mathcal{N}(0.85, 0.17)$		
	fit value	–	$1.04^{+0.18}_{-0.18}$	$1.23^{+0.18}_{-0.16}$	–	–
b_2	prior		$\mathcal{N}(0.33, 0.033)$	$\mathcal{N}(0.33, 0.033)$		
	fit value	–	$0.34^{+0.04}_{-0.03}$	$0.36^{+0.03}_{-0.04}$	–	–
b_{eff}	prior	[0.1, 10]			[0.1, 10]	[0.1, 10]
	fit value	$2.19^{+0.15}_{-0.14}$	–	–	$3.31^{+0.07}_{-0.07}$	$2.24^{+0.14}_{-0.15}$
χ^2/dof		1.90	1.76	1.52	1.63	1.88
AIC		169.36	157.06	136.56	145.36	167.94
BIC		171.85	164.52	144.03	147.85	170.43

tained using CMB lensing and LoTSS DR1 data. Considering redshift information dominantly determined by available photo- z information, we again obtain slightly higher bias values for the LoTSS DR1 galaxies (Case B). Considering different $N(z)$ templates and bias $b(z)$ forms, with MCMC sampler, we surprisingly find that the best fit result (best reduced- χ^2 , AIC, BIC) for Case C i.e. by assuming $N(z)$ given in Nusser & Tiwari (2015) and a quadratic bias form, although we obtain the bias value slighter higher. We add that the performance of our MCMC sample is verified by recovering model input bias, $b(z)$, by fitting pseudo- C_ℓ 's mean from mocks.

To compare our results with Siewert et al. (2020a), we have also given our measurements for 2PCF for our catalog. We obtain roughly the same results as in Siewert et al. (2020a). The 2PCF calculated for broad right ascension patches differ, this potentially indicates the large scale systematics in data. These large scale anomalies in real space clustering signal corresponds to low multipoles¹¹, roughly $l < 10$. For our fittings we have considered power spectrum above multipole $l = 100$.

¹¹ e.g. 20 degree scales roughly correspond to $l \approx \pi/\theta = 9$

9. CONCLUSION AND DISCUSSION

We have presented the detailed mocks and projected clustering statistics of point sources from LoTSS first data releases, based on the observation of 424 square degrees of the sky at $\sim 150\text{MHz}$. With simple 2-point correlation statistics, we notice somewhat different clustering in large right-ascension patches, presumably evincing the large-scale flux calibration systematics in data. The angular power spectrum C_ℓ , the spherical harmonic decomposition of the fluctuations in angular space, measurements efficiently separate the scale-dependent real space number density fluctuations, and we see a good match of LoTSS DR1 measured C_ℓ 's with standard ΛCDM theory. Although the LoTSS DR1 catalog appears to have significant large scale density systematises, the galaxy clustering measurements reveal cosmological results.

The LOFAR observations are at relatively low radio frequency and the strength of the systematic effects corrupting the data is significantly higher, and thus the calibration and source cataloging is challenging. Even so, the data calibration pipeline by Shimwell et al. (2019) sufficiently performs to deliver a reasonably work-

able source catalog and we are able to do large-scale cosmology with this. We encourage the LOFAR team to improve on flux calibration and cataloging, the next catalog will hopefully not have large scale flux calibration or issues as we see with DR1, e.g., the 2PCF over big sky patches will not differ! Furthermore, we need better estimates on redshifts, the present partial availability of photometric redshifts is not reliably representing the LoTSS population. Ideally, above LoTSS completeness limit we need accurate measurements for all galaxies over some small sky patch to obtain a complete redshift distribution of LoTSS galaxies. A narrow but sufficiently deep (reaching up to sub mJy flux limits of radio sources) spectroscopic or photometric redshift survey will help (Duncan et al. 2020). With improved calibrations, large sky coverage, and higher number density, the upcoming catalogs from LOFAR are expected to be a significant improvement over present existing low radio frequency radio catalogs, e.g., the TGSS from GMRT and GLEAM from MWA. The upcoming LoTSS catalogs are definitely an excellent opportunities for cosmological studies in the low radio frequency regime.

10. ACKNOWLEDGMENTS

We thank Thilo Siewert for helping with the LoTSS DR1 catalog and masks. PT acknowledges the support by the PIFI (Project No. 2019PM0007) program of the Chinese Academy of Sciences. PT, RZ, JZ and GBZ are supported by the National Key Basic Research and Development Program of China (No. 2018YFA0404503) and NSFC Grants 11925303 and 11720101004, and a grant of CAS Interdisciplinary Innovation Team. JZ is supported by Chinese Scholarship Council(CSC) and Science and Technology Facilities Council(STFC) for visiting University of Portsmouth.

LOFAR data products were provided by the LOFAR Surveys Key Science project (LSKSP; <https://lofar-surveys.org/>) and were derived from observations with the International LOFAR Telescope (ILT). LOFAR (van Haarlem et al. 2013) is the Low Frequency Array designed and constructed by ASTRON. It has observing, data processing, and data storage facilities in several countries, which are owned by various parties (each with their own funding sources), and which are collectively operated by the ILT foundation under a joint scientific policy. The efforts of the LSKSP have benefited from funding from the European Research Council, NOVA, NWO, CNRS-INSU, the SURF Co-operative, the UK Science and Technology Funding Council and the Jülich Supercomputing Centre.

REFERENCES

- Agarwal, A., Singh, N. K., Jain, P., & Tiwari, P. 2019, *Eur. Phys. J. C*, 79, 582
- Alonso, D., Bellini, E., Hale, C., Jarvis, M. J., & Schwarz, D. J. 2020, [arXiv:2009.01817](https://arxiv.org/abs/2009.01817)
- Alonso, D., Sanchez, J., & Slosar, A. 2019, *Mon. Not. Roy. Astron. Soc.*, 484, 4127
- Bengaly, C. A., Siewert, T. M., Schwarz, D. J., & Maartens, R. 2019, *Mon. Not. Roy. Astron. Soc.*, 486, 1350
- Bengaly, C. A. P., Maartens, R., & Santos, M. G. 2018, *JCAP*, 1804, 031
- Best, P. N., Kauffmann, G., Heckman, T. M., et al. 2005, *Monthly Notices of the Royal Astronomical Society*, 362, 25
- Best, P. N., Ker, L. M., Simpson, C., Rigby, E. E., & Sabater, J. 2014, *MNRAS*, 445, 955
- Calistro Rivera, G., Williams, W. L., Hardcastle, M. J., et al. 2017, *MNRAS*, 469, 3468
- Challinor, A., & Lewis, A. 2011, *Physical Review D*, 84, 043516
- Chen, S., & Schwarz, D. J. 2015, *Physical Review D*, 91, 043507
- Choudhuri, S., Ghosh, A., Roy, N., et al. 2020, *Mon. Not. Roy. Astron. Soc.*, 494, 1936
- Condon, J. J., Cotton, W. D., Greisen, E. W., et al. 1998, *AJ*, 115, 1693
- Cooray, A., & Sheth, R. 2002, *Physics Reports*, 372, 1
- Das, K. K., Sankharva, K., & Jain, P. 2021, [arXiv:2101.11016](https://arxiv.org/abs/2101.11016)
- de Oliveira-Costa, A., Tegmark, M., Zaldarriaga, M., & Hamilton, A. 2004, *PhRvD*, 69, 063516
- Dolfi, A., Branchini, E., Bilicki, M., et al. 2019, *A&A*, 623, A148
- Duncan, K. J., et al. 2019, *Astron. Astrophys.*, 622, A3
- Duncan, K. J., Kondapally, R., Brown, M. J. I., et al. 2020, [arXiv:2011.08204](https://arxiv.org/abs/2011.08204)
- Falcke, H. D., van Haarlem, M. P., de Bruyn, A. G., et al. 2007, *Highlights of Astronomy*, 14, 386
- Fanaroff, B. L., & Riley, J. M. 1974, *MNRAS*, 167, 31P
- Ghosh, S., Jain, P., Kashyap, G., et al. 2016, *Journal of Astrophysics and Astronomy*, 37, 1
- Girelli, G., Pozzetti, L., Bolzonella, M., et al. 2020, *Astron. Astrophys.*, 634, A135
- Hale, C. L., Jarvis, M. J., Delvecchio, I., et al. 2018, *MNRAS*, 474, 4133
- Hurley-Walker, N., Callingham, J. R., Hancock, P. J., et al. 2017, *MNRAS*, 464, 1146
- Intema, H. T., Jagannathan, P., Mooley, K. P., & Frail, D. A. 2017, *A&A*, 598, A78
- Jarvis, M., Bernstein, G., & Jain, B. 2004, *Monthly Notices of the Royal Astronomical Society*, 352, 338
- Kauffmann, G., Heckman, T. M., Tremonti, C., et al. 2003, *MNRAS*, 346, 1055
- Krumpe, M., Miyaji, T., Coil, A. L., & Aceves, H. 2018, *MNRAS*, 474, 1773
- Lan, T.-W., & Prochaska, J. X. 2021, *MNRAS*, [arXiv:2009.04482](https://arxiv.org/abs/2009.04482)
- Lewis, A. 2013, *Phys. Rev.*, D87, 103529
- Lewis, A., & Bridle, S. 2002, *Phys. Rev.*, D66, 103511
- Ma, C.-P., & Fry, J. N. 2000, *ApJ*, 543, 503
- Maartens, R., Clarkson, C., & Chen, S. 2018, *JCAP*, 01, 013
- Mandelbaum, R., Li, C., Kauffmann, G., & White, S. D. 2009, *Mon. Not. Roy. Astron. Soc.*, 393, 377
- Mandelbaum, R., Li, C., Kauffmann, G., & White, S. D. M. 2009, *MNRAS*, 393, 377
- Mo, H., & White, S. D. 1996, *Mon. Not. Roy. Astron. Soc.*, 282, 347

- Navarro, J. F., Frenk, C. S., & White, S. D. M. 1997, *ApJ*, 490, 493
- Nusser, A., & Tiwari, P. 2015, *ApJ*, 812, 85
- Planck Collaboration, Aghanim, N., Akrami, Y., et al. 2018, arXiv:1807.06209
- Press, W. H., & Schechter, P. 1974, *ApJ*, 187, 425
- Qiang, D.-C., Deng, H.-K., & Wei, H. 2020, *Class. Quant. Grav.*, 37, 185022
- Ralston, J. P., & Jain, P. 2004, *IJMPD*, 13, 1857
- Rana, S., & Bagla, J. S. 2019, *MNRAS*, 485, 5891
- Röttgering, H., de Bruyn, A. G., Fender, R. P., et al. 2003, in *Texas in Tuscany. XXI Symposium on Relativistic Astrophysics*, ed. R. Bandiera, R. Maiolino, & F. Mannucci, 69–76
- Röttgering, H., van Haarlem, M., & Miley, G. 2005, in *IAU Colloq. 199: Probing Galaxies through Quasar Absorption Lines*, ed. P. Williams, C.-G. Shu, & B. Menard, 381–386
- Rubart, M., & Schwarz, D. J. 2013, *A&A*, 555, arXiv:1301.5559
- Scherrer, R. J., & Bertschinger, E. 1991, *ApJ*, 381, 349
- Schwarz, D. J., Starkman, G. D., Huterer, D., & Copi, C. J. 2004, *PhRvL*, 93, 221301
- Scoccimarro, R., Sheth, R. K., Hui, L., & Jain, B. 2001, *ApJ*, 546, 20
- Secrest, N. J., von Hausegger, S., Rameez, M., et al. 2020, arXiv:2009.14826
- Seljak, U. 2000, *MNRAS*, 318, 203
- Shimwell, T. W., Röttgering, H. J. A., Best, P. N., et al. 2017, *A&A*, 598, A104
- Shimwell, T. W., Tasse, C., Hardcastle, M. J., et al. 2019, *A&A*, 622, A1
- Siewert, T., et al. 2020a, *Astron. Astrophys.*, 643, A100
- Siewert, T. M., Schmidt-Rubart, M., & Schwarz, D. J. 2020b, arXiv:2010.08366
- Singal, A. K. 2011, *ApJL*, 742, L23
- Smith, D. J. B., Best, P. N., Duncan, K. J., et al. 2016, in *SF2A-2016: Proceedings of the Annual meeting of the French Society of Astronomy and Astrophysics*, ed. C. Reylé, J. Richard, L. Cambrésy, M. Deleuil, E. Pécontal, L. Tresse, & I. Vauglin, 271–280
- Tiwari, P. 2019, *Res. Astron. Astrophys.*, 19, 096
- Tiwari, P., & Aluri, P. K. 2019, *Astrophys. J.*, 878, 32
- Tiwari, P., Ghosh, S., & Jain, P. 2019, *Astrophys. J.*, 887, 175
- Tiwari, P., & Jain, P. 2015, *MNRAS*, 447, 2658
- Tiwari, P., Kothari, R., Naskar, A., Nadkarni-Ghosh, S., & Jain, P. 2015, *Astroparticle Physics*, 61, 1
- Tiwari, P., & Nusser, A. 2016, *Journal of Cosmology and Astroparticle Physics*, 2016, 062
- Torrado, J., & Lewis, A. 2020, arXiv:2005.05290
- van Haarlem, M. P. 2005, in *EAS Publications Series, Vol. 15*, *EAS Publications Series*, ed. L. I. Gurvits, S. Frey, & S. Rawlings, 431–444
- van Haarlem, M. P., Wise, M. W., Gunst, A. W., et al. 2013, *A&A*, 556, A2
- Williams, W. L., Hardcastle, M. J., Best, P. N., et al. 2019, *A&A*, 622, A2
- Wilman, R. J., Miller, L., Jarvis, M. J., et al. 2008, *MNRAS*, 388, 1335
- Wolf, J., Nandra, K., Salvato, M., et al. 2021, arXiv e-prints, arXiv:2101.05585
- Xavier, H. S., Abdalla, F. B., & Joachimi, B. 2016, *Mon. Not. Roy. Astron. Soc.*, 459, 3693